Selenium and selenium-sulfur cathode materials for high-energy rechargeable magnesium batteries

Zhirong Zhao-Karger [a, *], Xiu-Mei Lin [b], Christian Bonatto Minella [a], Di Wang [a], Thomas Diemant [c], R. Jürgen Behm [b, c], Maximilian Fichtner [a, b]

[a] Institute of Nanotechnology, Karlsruhe Institute of Technology (KIT), Hermann-von-Helmholtz-Platz 1, 76344 Eggenstein-Leopoldshafen, Germany
[b] Helmholtz Institute Ulm for Electrochemical Energy Storage (HIU), Karlsruhe Institute of Technology (KIT), Helmholtzstr.11, 89081 Ulm, Germany
[c] Institute of Surface Chemistry and Catalysis, Ulm University, Albert-Einstein-Allee 47, 89081 Ulm, Germany

HIGHLIGHTS

- Selenium based composites are studied as cathode materials for magnesium batteries.
- The selenium composites show high volumetric capacity and rate capability.
- The electrochemical mechanism of Mg Se battery is investigated.

ARTICLE INFO

Keywords:
Rechargeable Mg battery
Selenium cathode
Selenium-sulfur cathode
Electrochemical reactions

ABSTRACT

Magnesium (Mg) is an attractive metallic anode material for next generation batteries owing to its inherent dendrite free electrodeposition, high capacity and low cost. Here we report a new class of Mg batteries based on both elemental selenium (Se) and selenium sulfur solid solution (SeS_2) cathode materials. Elemental Se confined into a mesoporous carbon was used as a cathode material. Coupling the Se cathode with a metallic Mg anode in a non nucleophilic electrolyte, the Se cathode delivered a high initial volumetric discharge capacity of 1689 mA h cm ^{3} and a reversible capacity of 480 mA h cm ^{3} was retained after 50 cycles at a high current density of 2 C. The mechanistic insights into the electrochemical conversion in Mg Se batteries were investigated by microscopic and spectroscopic methods. The structural transformation of cyclic Se_8 into chainlike Se_n upon battery cycling was revealed by *ex situ* Raman spectroscopy. In addition, the promising battery performance with a SeS_2 cathode envisages the perspective of a series of SeS_n cathode materials combining the benefits of both selenium and sulfur for high energy Mg batteries.

1. Introduction

New battery systems with high energy density are being extensively explored in order to meet the demand of rapidly developing market for longer lasting portable electronics and electric vehicles (EVs). It is recognized that the conventional lithium ion batteries (LIBs) are approaching their theoretical energy density limits and the issues of safety and high cost remain unre solved [1–3]. Rechargeable Mg batteries have been recognized as an attractive alternative for energy storage owing to the inherent merits of Mg metal as anode in terms of high volumetric capacity (3837 mA h cm^{-3}), dendrite free deposition and low cost [4–6]. However, Mg batteries are hampered by several technical obstacles, such as the lack of electrolyte which is stable in contact with the electrode materials and the quest for practical cathodes offering high accessible capacity and rate capability. In fact, there are a few types of conventional intercalation materials capable of storing Mg^{2+} ions reversibly due to the intrinsically sluggish Mg^{2+} ion diffusion kinetics in the cathode hosts [7]. Thus, the challenges to realize the rechargeable Mg battery technology are not only the improvement of the electrolyte towards high oxidative stability, but also the discovery of practically cathode materials enabling high performance of Mg batteries.

Recent achievements of non nucleophilic electrolytes with good electrochemical performance have paved the way to employ

* Corresponding author.
E-mail address: zhirong.zhao-karger@kit.edu (Z. Zhao-Karger).

conversion cathode materials for advanced high energy magnesium batteries [8–10]. Beyond intercalation chemistry, sulfur is an attractive cathode material with a high theoretical capacity, low cost and non toxicity. The volumetric energy density of the couple of a sulfur cathode and a Mg anode can theoretically reaches up to 3200 Wh l^{-1}. The non nucleophilic electrolytes developed in our laboratory through the reaction between magnesium bis(hexamethyldisilazide) [$(HMDS)_2Mg$] and aluminum chloride ($AlCl_3$) in different ethers have been successfully applied to the magnesium sulfur (Mg–S) batteries [11,12]. Despite the considerable achievements, the Mg–S batteries still suffer from capacity fading upon cycling mainly due to the dissolution of long chain magnesium polysulfide (MgS_n, $n \geq 4$). While making an effort to address these issues by the fabrication of new S cathode materials [13], we are also attempting to explore new electrode materials for advanced Mg battery systems.

Selenium (Se), a *d* electron containing element in Group 16, is proposed as a prospective electrode material, which is chemically similar to S and possesses some merits beyond S. In spite of its lower gravimetric capacity (about 678 mA h g^{-1}) compared to S (1675 mA h g^{-1}), the theoretical volumetric capacity of Se (3268 mA h cm^{-3}) is comparable to that of S (3467 mA h cm^{-3}). More importantly, Se has an electronic conductivity of 1×10^{-3} S m^{-1}, approximately 20 orders of magnitude higher than S (5×10^{-28} S m^{-1}) [14]. It is expected that Se based electrodes could bring about higher electrochemical reactivity, better rate capability and greater accessible capacity compared with S in a battery system. In addition, the miscibility of Se and S gives rise to numerous solid solutions in forms of cyclic Se_nS_{8-n} and Se_nS_{12-n} molecules [15,16]. which can be potential cathode materials in a battery system. The gravimetric capacity and energy density of the SeS_n cathodes will be accordingly increased with the contribution of S while enhanced electrical conductivity will be offered by Se. Recently, Se based materials have been intensively investigated as potential cathode candidates for high performance rechargeable Li and Na batteries [17–23]. Particularly, it has been reported that the addition of a small amount of selenium to the sulfur cathode material could effectively diminish the problem with the polysulfide shuttle in Li–S batteries [21]. The couple of Se as cathode and Mg as anode has been supposed to be an ideal combination for electrochemical energy storage [23], however, the electrochemistry of Mg–Se battery remains unexplored. Herein, we investigate for the first time the potential of Se and SeS_2 as cathode materials for rechargeable magnesium batteries. Besides the development of high performance Mg batteries, this study is also aimed at enhancing the fundamental understanding of the electrochemistry between Mg and chalcogens.

2. Experimental

The chemical operations were either carried out on the bench under Ar (99.9999%) using standard Schlenk techniques, or in an argon filled glove MBraun glove box with recirculation system and water and oxygen concentrations below 0.1 ppm. The chemicals including anhydrous solvents, magnesium bis(hexamethyldisilazide) [$(HMDS)_2Mg$, 97%], magnesium chloride (99%) and sodium alginate were purchased from Sigma Aldrich. Mesoporous carbon material CMK 3 was provided by Nanjing XFNANO Materials. Selenium (Se), selenium disulfide (SeS_2) and Mg powder (99.6%) were purchased from Alfa Aesar.

2.1. Material synthesis and characterization

2.1.1. Electrolyte preparation

The non nucleophilic electrolyte (denoted as Mg HMDS) was synthesized according to the previous procedures [11], but using a mixture of tetraglyme and diglyme in a volumetric ratio of 1:1 as solvents in order to lower the viscosity of the electrolyte.

2.1.2. Preparation of SeCMK 3 composite

CMK 3 (0.5 g) and selenium (1.2 g) were ball milled in a silicon nitride jar filled with silicon nitride balls, with a ball to powder ratio of 20:1 at 200 rpm for 10 h. The mixture was subsequently heated in a closed quartz tube with a rotating furnace at 260 °C under argon for 16 h.

2.1.3. Preparation of SeS_2CMK 3 composite

CMK 3 (0.5 g) and SeS_2 (1.2 g) were ball milled in a silicon nitride jar with a ball to powder weight ratio of 20:1 at 200 rpm for 10 h. The mixture was subsequently heated in an autoclave at 160 °C for 20 h.

2.1.4. Solid state synthesis of MgSe

MgSe was prepared by ball milling a mixture of Se (0.02 mol, 1.58 g) and Mg (0.02 mol, 0.48 g) in a silicon nitride jar with a ball to powder weight ratio of 20:1 at 400 rpm for 20 h.

2.2. Material characterization

Powder X ray Diffraction (XRD) patterns were recorded in the 2θ range of 10–75° using a Philips X'pert diffractometer equipped with Cu Kα source. Transition electron microscopy (TEM) was performed on a FEI Titan 80–300 Transmission Electron Microscope operated at an accelerating voltage of 300 kV. Scanning transmission electron microscopy (STEM) images were acquired with a high angle annular dark field (HAADF) detector (Fischione Instruments). The energy dispersive X ray (EDX) spectra were acquired by an EDAX SUTW EDX detector. Scanning electron microscopy (SEM) images were acquired with a Zeiss ultra plus electron scanning microscope.

X ray Photoelectron Spectroscopy (XPS) measurements were performed using a PHI 5800 MultiTechnique ESCA system (Physical Electronic). To avoid surface contamination, the samples were transferred under an inert gas atmosphere to the sample load lock of the XPS system. The samples were neutralized with electrons from a flood gun (current 3 μA) to compensate for charging effects at the surface. The spectra were acquired using monochromatized Al Kα (1486.6 eV) radiation. The measurements were performed at a detection angle of 45°, with pass energies at the analyzer of 93.9 eV and 29.35 eV for survey and detail scans, respectively. The main C 1s peak was used as binding energy (BE) reference. For the electrode materials, which contain CMK 3, the BE of the main C1s peak was set to 284.5 eV. In the case of the reference compounds (pristine Se and MgSe without CMK 3), the peak of adventitious C (at 284.8 eV) was used.

Raman measurements were carried out with a confocal Raman microscope (InVia Renishaw) in the spectral range of 200–2000 cm^{-1} using a 633 nm laser excitation source.

Thermogravimetric analysis (TGA) of the samples was carried out simultaneously with differential scanning calorimetry (DSC) using a Setaram thermal analyzer SENSYS evo instrument. The measurements were conducted from room temperature to 600 °C under helium flow (20 ml min^{-1}) at a heating rate of 10 °C min^{-1}.

The surface area and porosity of the materials were analyzed with the Brunauer Emmett Teller (BET) methods and the physisorption isotherms were collected on a Micromeritics ASAP 2020 instrument by applying nitrogen gas at liquid nitrogen temperature. Prior to the measurement, the samples were degassed for 24 h at 200 °C for the carbon material and at 70 °C for the composites. Pore size distributions (PSD) were calculated using BJH methods.

2.3. Electrochemical measurements

The cathode electrodes were prepared by mixing 80 wt% of SeCMK 3 composite with 15 wt% Super P carbon (TIMCAL) in 5 wt% sodium alginate (SA) dissolved in water. The slurry was uniformly coated over an Inconel 625 current collector [24], subsequently dried at 80 °C for 24 h. Electrochemical measurements were con ducted using a Swagelok cell with SeCMK 3 or SeS_2CMK 3 as a cathode electrode, Mg foil as an anode electrode, a Whatman glass fiber sheet as separator and Mg HMDS electrolyte. The assembly of the cells was conducted in an argon filled MBRAUN glove box with water and oxygen concentrations below 0.1 ppm. The cells were placed in an incubator to maintain a constant temperature of 25 ± 0.1 °C. Galvanostatic charge–discharge measurements were performed using an Arbin battery tester. Cyclic voltammetry (CV) measurements were conducted using a Biologic VMP 3 potentiostat.

3. Results and discussion

Se exists in several allotropes and the most stable form is trigonal (gray) Se with a lattice consisting of helical chains arranged in a hexagonal array [25,26]. As shown in Fig. 1a, no reflection of the bulk crystalline trigonal Se is present in the XRD patterns of the SeCMK 3 composite indicating the uniform dispersion of Se in CMK 3. STEM image of SeCMK 3 in Fig. 1b shows the ordered channel structure of CMK 3 but also no crystalline Se. Elemental mapping of Se and carbon reveals a homogeneous distribution of Se in CMK 3 (Fig. 1c,d) and EDX analysis of SeCMK 3 confirms the presence of Se (Fig. 1e). The Se content in the composite was determined to be 50 wt% by thermogravimetric analysis (TGA) (Fig. S1). The surface and pore size analysis using Brunauer Emmett Teller (BET) methods reveals a significant decrease in both surface area (from 1083 $m^2\ g^{-1}$ for CMK 3 to 115 $m^2\ g^{-1}$ for SeCMK 3) and pore volume (from 1.2 for CMK 3 to 0.18 $cm^3\ g^{-1}$ for SeCMK 3). The change of pore size distribution in the pore region of 3–4 nm of CMK 3 and the composite SeCMK 3 shown in Fig. 1f indicates the confinement of Se within channels of the carbon scaffold. The structural change of Se in the composite was further characterized by Raman spectroscopy and will be discussed later in the text.

In this work, the non nucleophilic electrolyte (denoted as Mg HMDS) was employed for Mg–Se batteries because of its non nucleophilicity and compatibility with the S cathode [9,11]. The battery cycling was performed by galvanostatic methods. The values of the cell capacity are based on the mass of Se and the current rate of 1 C corresponds to the conversion of 1 Mg^{2+} ion per Se atom in 1 h at an equivalent capacity of 678 mA h g^{-1}. The redox reactions between Se and Mg were characterized by cyclic vol tammetry (CV). The cyclic voltammograms of the first three cycles at a scan rate of 0.05 mV s^{-1} from 0.5 to 2.6 V are shown in Fig. 2a. The first sweeping scan shows a sharp cathodic peak at about 1.2 V with a small shoulder and two anodic peaks at 1.8 and 2.4 V, which are associated with the reduction and subsequent re oxidation of Se, respectively. We suppose that the overall redox reaction in Mg–Se cell is: $Se + Mg^{2+} + 2e^- \leftrightarrow MgSe$. The strong peaks with small shoulders in the cyclic voltammograms indicate that the discharge of the Se cathode proceeds through multistep, which is also clearly displayed in the discharge/charge profiles of the Mg–Se cells operated at a low current rate of 20 mA g^{-1}(Se) as shown in Fig. S2. It is likely that reversible transformation between elemental Se and MgSe proceeds via intermediate phases. Similar to the sulfur system, during discharge, Se is reduced to soluble long chain pol yselenides Se_n^{2-} ($n > 4$) [27], and then further reduced to $MgSe_2$ and MgSe. In the subsequent cycles, the anodic peak shifts to a higher potential. The possible reasons for the shift will be the further discussed with the detailed spectroscopic characterizations.

The galvanostatic discharge and charge of SeCMK 3 as cathode for Mg–Se batteries were performed in the voltage region of 0.8–2.5 V at a current rate of 0.2 C. As shown in Fig. 2b, a well

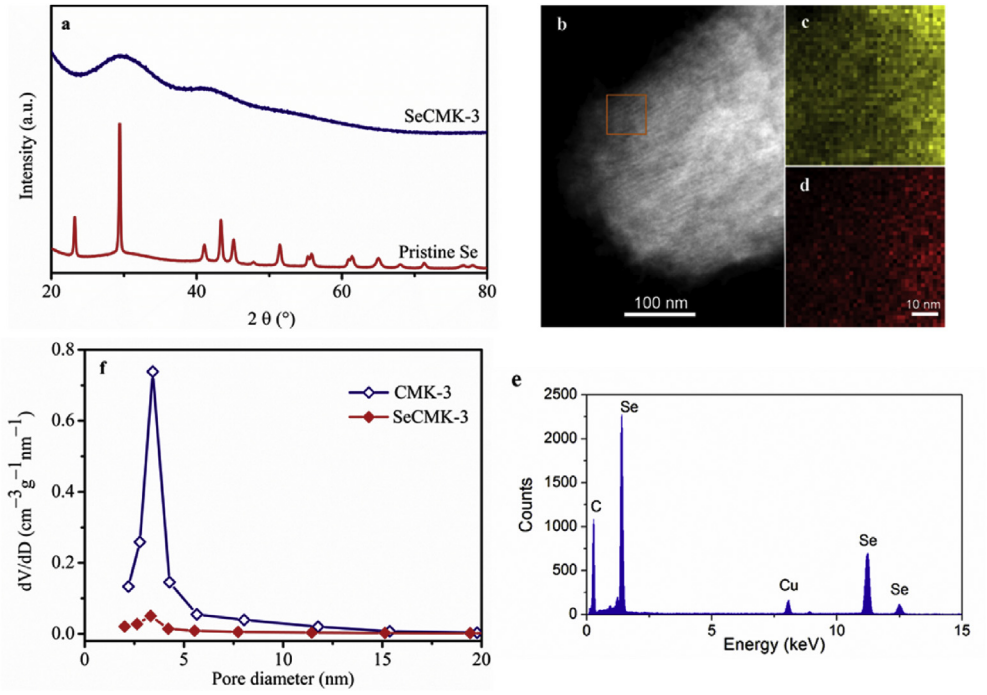

Fig. 1. (a) XRD patterns of Se and SeCMK-3, (b) STEM overview image of SeCMK-3, (c) mapping image of Se, (d) mapping image of carbon, (e) EDX pattern of SeCMK-3, (f) pore size distribution of CMK-3 and SeCMK-3.

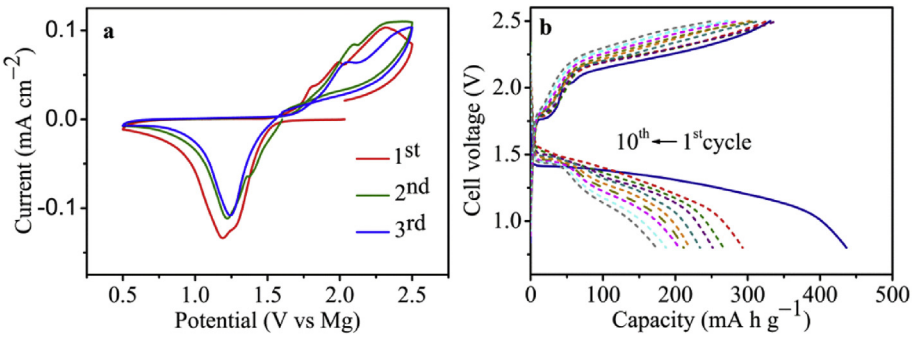

Fig. 2. (a) CV curves of Mg Se cell at a scan rate of 0.05 mV s ^{1}, (b) discharge/charge profiles of the cell at 0.2 C in the voltage range of 0.8 2.5 V in the initial 10 cycles.

defined voltage plateaus is presented at about 1.4 V, delivering a specific capacity of 460 mA h g^{-1}. The voltage plateaus persist in the discharge profiles upon cycling, but they are slightly shifted to a higher potential, which is consistent with the right shifting of the cathodic peaks in the cyclic voltammograms. The origin of the elevated discharge voltage will be discussed later in the paper. The initial charge curve exhibits two voltage steps corresponding to the two anodic peaks in CV, which might be indicative of the formation of $MgSe_n$ intermediates as mentioned above.

The cycling stability and rate capability of the Mg–Se cells were further investigated. As shown in Fig. 3a, the initial discharge profiles at a varied current density from 0.2 to 3 C exhibit similar apparent voltage plateaus at about 1.4 V, but the plateau region becomes shorter by increasing the current rate. The achievable capacity gradually drops with increased current rate, which is ex pected; nevertheless, a capacity of 320 mA h g^{-1} was still achieved at a high current rate of 3 C indicating a fast kinetics of the mag nesiation process in the Mg–Se cells. This may be attributed to the good electrical conductivity of elemental Se. In contrast to the discharge profile with two apparent voltage plateaus of Mg–S batteries [11], the multi step discharge behavior in Mg–Se batteries likely trend towards a single voltage plateau. This may imply that the transformation of high order polyselenides to low order sele nides is faster than that of the polysulfides in Mg–S battery. The large hysteresis between discharge and charge potential may reflect the inherent kinetic limitation during the de magnesiation process in the Mg–Se batteries. On the other hand, the chemical change of Mg HMDS electrolyte and passivation of Mg anode caused by the dissolved polyselenides should also be taken into account, which will be further discussed. The extended cycling performance of the Mg–Se cells was evaluated. As shown in Fig. 3b, a reversible capacity of 100 mA h g^{-1} was retained after 50 cycles at a current rate of 2 C, which is superior to those obtained at low current rates. It might imply that high rate conditions lead to a suppression of the dissolution of polyselenides by shortening their retention time before the transformation into the final discharge product MgSe. It is noteworthy that the volumetric energy density of an energy storage system is of particular importance for portable devices and EVs because of the limited battery packing space. Owing to the high volumetric capacity density of both electrodes,

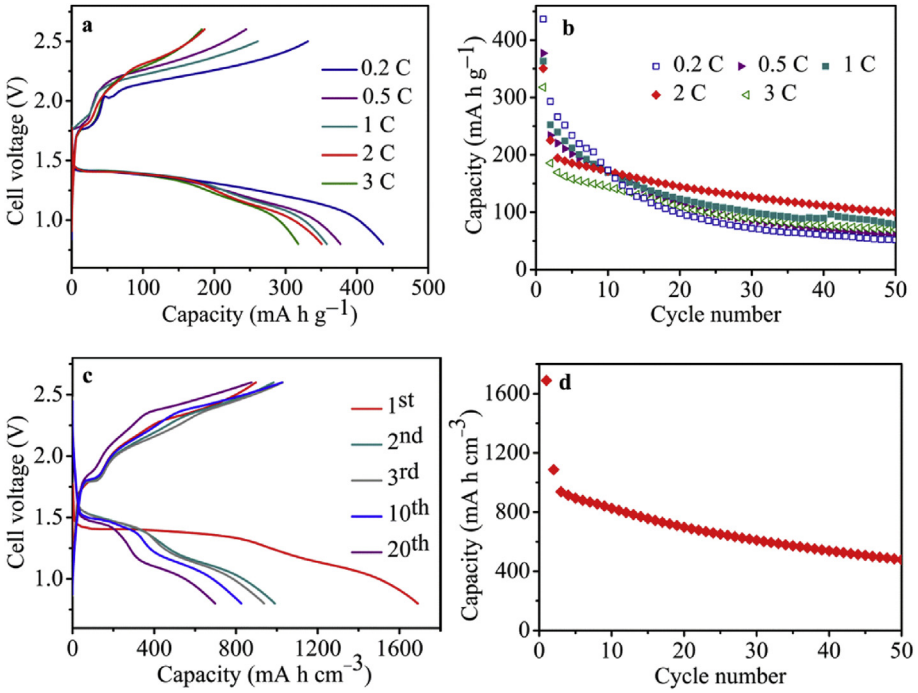

Fig. 3. (a) Galvanostatic discharge/charge profiles of the Mg Se cells at different C-rates in the voltage range of 0.8 2.8 V, (b) cycling performance of the Mg Se cells at different C-rates, (c) discharge/charge curves in the selected cycles at a rate of 2 C, (d) reversible volumetric capacity of SeCMK-3 at 2 C.

the couple of Se as cathode and Mg as anode is supposed to be "gold partners" for electrochemical energy storage in terms of high volumetric capacity and energy density [23]. Fig. 3c presents the discharge/charge profiles of the Mg–Se cell at a rate of 2 C. A volumetric capacity of 480 mA h cm^{-3} in was retained after 50 cycles as shown in Fig. 3d, which corresponds an energy density of 624 W h cm^{-3} with an average potential of 1.3 V.

The reaction mechanism in the new Mg–Se system is of fundamental importance to understand the battery chemistry. Therefore, the chemical composition of the cathode material at different discharge/charge states was further analyzed by *ex situ* X ray Photoelectron Spectroscopy (XPS) and Raman spectroscopy. The cathode samples were recovered from the Mg–Se cells after first discharge and first charge at a current rate of 20 mA g^{-1} to ensure the complement of the electrochemical conversion. Fig. 4a shows the discharge charge profile of the Mg–Se cells, in which the hysteresis was mitigated by applying a low current rate compared to the aforementioned battery performance at higher current rates.

The XPS analysis provided valuable information about the re action products on the cathode surface from the Mg–Se cell. We derived high resolution Se 3d and Mg 2p XPS spectra of the Se cathodes at various electrochemical states. The C 1s peak position of adventitious carbon at 284.8 eV was used as an internal refer ence. As the reference material, MgSe was synthesized by ball milling and characterized by XRD as shown in Fig. S3. The XPS spectra of the pristine Se and MgSe were recorded (Fig. S4). The Se 3d and Mg 2p XPS spectra after fitting are shown in Fig. 4b. Although the XPS signals of Mg 2p and Se 3d overlap, it can be used as additional evidence for the Se phase evolution during discharge and charge. For the initial SeCMK 3 cathode, Se $3d_{5/2}$ and $3d_{3/2}$ peaks located at ~55.3 and ~56.2 eV, with a spin orbit splitting of 0.86 eV shown in spectrum 1 have been attributed to metallic se lenium. In Fig. 4b, curve 2 displays the Se 3d XPS spectra for the product discharged to 1.2 V, in which the Se $3d_{5/2}$ peak moves to ward lower binding energy (at about 55.6 eV) indicating the elec trochemical reduction of Se with the formation of $MgSe_n$ [28–30]. After discharge to 0.5 V, as shown in curve 3, the Se $3d_{5/2}$ peak further shifts to lower binding energy while the intensity of Mg 2p peak at 57.2 eV is enhanced. The formation of the MgSe and $MgSe_2$ as the final discharge products may be confirmed on the basis of

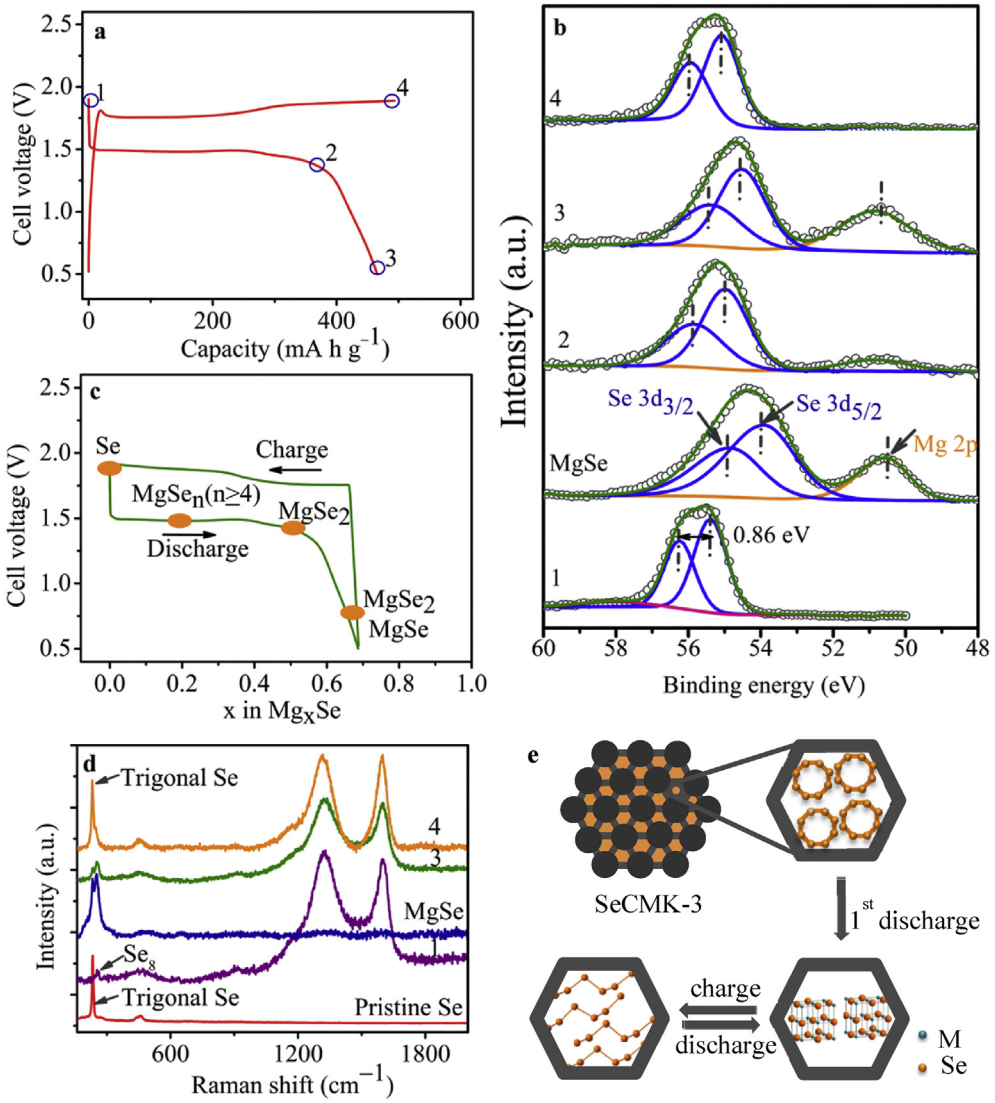

Fig. 4. (a) Discharge/charge curve of the SeCMK-3 electrode at 20 mA g^{-1} in the first cycle; (b) XPS spectra of the Se cathode at different electrochemical states as marked in the discharge/charge curve in (a); (c) Proposed Se phase evolution during the electrochemical reaction of the Mg/SeCMK-3 cell in the Mg-HMDS electrolyte; (d) Raman spectra of the Se cathode at different electrochemical states as marked in the discharge/charge curve in (a); (e) Proposed phase transformation of the SeCMK-3 cathode during discharge/charge.

both the spectra of MgSe reference and the achieved capacity of about 470 mA h g^{-1}, which corresponds to the conversion of approximately 0.7 Mg atom per Se atom. Upon charging, the Mg 2p signals from MgSe completely disappear, and the Se 3p peaks move back to the binding energy of metallic Se (curve 4 in Fig. 4b), sug gesting that MgSe and $MgSe_2$ are reversibly oxidized to Se. These results not only confirm the reversible electrochemical conversion reaction between Se and Mg, but also reveal the occurrence of the polyselenides as intermediate products in the Mg–Se batteries. A proposed phase evolution of the Se cathode with a Mg anode in the electrolyte Mg HMDS is displayed in Fig. 4c.

We have further investigated the structural and phase changes of Se induced by the confinement within the porous carbon matrix and the electrochemical reactions by means of Raman spectros copy. As shown in Fig. 4d, the crystalline Se exhibits the charac teristic Raman shift at 233 cm^{-1} [31,32], which is attributed to the first order A_1 symmetric bond stretching modes of trigonal Se–Se bonds. A blue shift to 257 cm^{-1} presented in the Raman spectrum 1 for the SeCMK 3 composite corresponds to the cyclic Se_8 molecules [33], implying that the Se chains were converted into cyclic Se_8 inside the pores of CMK 3 by the melt diffusion.

After the first discharge to 0.5 V, the transformation from Se to MgSe was confirmed by comparing the Raman spectrum 3 with the spectrum of the MgSe reference compound (Fig. 4d). During the charging process, interestingly, the chain like Se_n was formed instead of cyclic Se_8 within the mesopores of CMK 3, which is inferred from the corresponding vibrations at 233 cm^{-1}; the broadness of the signal reflects the disorder of the Se_n chains, probably due to the space constraints in the narrow region of the pores. Fig. 4e illustrates the phase transformation of the SeCMK 3 cathode during discharge/charge, namely the cyclic Se_8 molecules encapsulated in the carbon matrix after the heat treatment convert to chain like Se_n molecules in the initial discharge/charge cycle and persist in their chain structure in the subsequent reversible con versions. This kind of phase transformation phenomena has also been observed in the Li–Se batteries [18]. It is noteworthy that Se is thermodynamically stable as chains, which is distinctive from the S that is more stable as rings. This may also explain the preference of the chain structure rather than ring structure of Se through the electrochemical oxidation of MgSe. Moreover, the Se_8 rings are electrical insulating whereas Se with chain structure possesses good conductivity [34], which is beneficial to facilitate the redox reactions in a battery system.

To gain more insights into the origin of the irreversible capacity in the first cycle and the capacity fading upon cycling, we also performed the post mortem study on the Mg–Se cells at various cycling stages. The scanning electron microscopy (SEM) images and EDX spectra show no evidence of morphological change of the Mg foil soaked in the Mg HMDS electrolyte for two weeks, confirming the chemical stability of the electrolyte against metallic Mg. After the first discharge, an apparent surface coarsening of the Mg foil from the disassembled cell was revealed by SEM (Fig. S5). Since no other element except Mg was detected by EDX, we suppose that the morphologic change of Mg anode is merely caused by the electro chemical stripping of Mg in the electrolyte. The images of Mg anode taken from the cells at various cycling states show a small amount of $MgCl_2$ deposited on the surface of Mg foil after the first charge process and the quantity of $MgCl_2$ enhances progressively in the subsequent cycles. The evidence of the reddish color of the glass fiber separator after 20 cycles, verifies the dissolution of the poly selenide in the electrolyte. The polyselenides might also disturb the equilibria in the electrolyte, which leads to the $MgCl_2$ aggregates on the Mg anode and consequently impede the reversible Mg plating. So the suppression of the polyselenide still appears to be the pre requisite for further performance improvement of Mg–Se batteries.

Preliminary investigation of one SeS_n based system was carried out with SeS_2CMK 3 composite as cathode material. The cell composed of the SeS_2 cathode and a Mg anode in the Mg HMDS electrolyte was discharged to a cut off potential of 0.5 V and sub sequently charged to 2.5 V at a current rate of 40 mA g^{-1} and maintained at 2.5 V until reaching a capacity of 650 mA h g^{-1} (The charge profiles are shown in Fig. S6). The initial discharge profile exhibits two well defined voltage plateaus at 1.46 V and 1.18 V, respectively, delivering an initial capacity of about 600 mA h g^{-1} (Fig. 5), which is higher than that offered by the SeCMK 3 cathode.

As Se and S are miscible, many readily available solid solution compounds represent a broad class of new cathode materials with higher theoretical capacities than Se alone and superior electrical conductivity to S alone. Additionally, the higher cost owing to the lower abundance of Se could be compensated by using SeS_n solid solutions as electrode materials for the commercialization of the battery systems. These preliminary results encourage further dis covery and optimization of Se based materials for high energy rechargeable Mg batteries.

4. Conclusions

Elemental Se confined in ordered mesoporous carbon by a melt diffusion method was studied as cathode material for rechargeable Mg batteries. The SeCMK 3 composite as a cathode exhibits a discharge voltage plateau at about 1.4 V with good reversibility and rate performance. The electrochemical mechanism has been investigated and it suggests that the conversion between the se lenium cathode and the Mg anode proceeds via the polyselenide intermediate phases in the ethereal solution of the non nucleophilic electrolyte. Complementary characterization by Raman spectroscopy revealed that the cyclic Se_8 molecules in the pore structure transform into the trigonal phase with Se_n chains during the reversible electrochemical reaction. The polyselenide dissolution was observed, which might be responsible for the ca pacity fading of the Mg–Se batteries and could be further mitigated by applying advanced cathode fabrications. Furthermore, SeS_n solid solution compounds offer the opportunity to combine the merits of both Se and S and optimize the SeS_n based cathode materials with good conductivity and high energy density for rechargeable Mg batteries. The battery performance of the SeS_2 cathode material highlights the perspectives of a new class of SeS_n cathode materials for high energy Mg batteries.

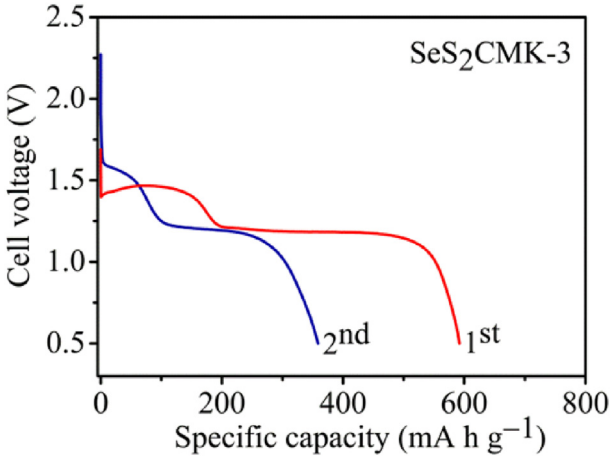

Fig. 5. Discharge profiles of the SeS_2 cathode in the initial 2 cycles in a Mg-based cell.

Appendix A. Supplementary data

Supplementary data related to this article can be found at http://dx.doi.org/10.1016/j.jpowsour.2016.05.034.

References

[1] A. Manthiram, Materials challenges and opportunities of lithium ion batteries, J. Phys. Chem. Lett. 2 (2011) 176 184.
[2] N.S. Choi, Z. Chen, S.A. Freunberger, X. Ji, Y.-K. Sun, K. Amine, G. Yushin, L.F. Nazar, J. Cho, P.G. Bruce, Challenges facing lithium batteries and electrical double-layer capacitors, Angew. Chem. Int. Ed. 51 (2012) 9994 10024.
[3] H.D. Yoo, E. Markevich, G. Salitra, D. Sharon, D. Aurbach, On the challenge of developing advanced technologies for electrochemical energy storage and conversion, Mater. Today 17 (2014) 110 121.
[4] T.D. Gregory, R.J. Hoffman, R.C. Winterton, Nonaqueous electrochemistry of magnesium, J. Electrochem. Soc. 137 (1990) 775 780.
[5] D. Aurbach, Y. Cohen, M. Moshkovich, The study of reversible magnesium deposition by in situ scanning tunneling microscopy, Electrochem. Solid-State Lett. 4 (2001) A113 A116.
[6] M. Jackle, A. Groß, Microscopic properties of lithium, sodium, and magnesium battery anode materials related to possible dendrite growth, J. Chem. Phys. 141 (2014) 174710 174717.
[7] H.D. Yoo, I. Shterenberg, Y. Gofer, G. Gershinsky, N. Pour, D. Aurbach, Mg rechargeable batteries: an on-going challenge, Energy. Environ. Sci. 6 (2013) 2265 2279.
[8] H.S. Kim, T.S. Arthur, G.D. Allred, J. Zajicek, J.G. Newman, A.E. Rodnyansky, A.G. Oliver, W.C. Boggess, J. Muldoon, Structure and compatibility of a magnesium electrolyte with a sulphur cathode, Nat. Commun. 2 (2011) 427.
[9] Z. Zhao-Karger, X. Zhao, O. Fuhr, M. Fichtner, Bisamide based non-nucleophilic electrolytes for rechargeable magnesium batteries, RSC Adv. 3 (2013) 16330 16335.
[10] O. Tutusaus, R. Mohtadi, T.S. Arthur, F. Mizuno, E.G. Nelson, Y.V. Sevryugina, An efficient halogen-free electrolyte for use in rechargeable magnesium batteries, Angew. Chem. Int. Ed. 54 (2015) 7900 7904.
[11] Z. Zhao-Karger, X. Zhao, D. Wang, T. Diemant, R.J. Behm, M. Fichtner, Performance improvement of magnesium sulfur batteries with modified non-nucleophilic electrolytes, Adv. Energy Mater. 5 (2015) 1401155.
[12] T. Gao, M. Noked, A.J. Pearse, E. Gillette, X. Fan, Y. Zhu, C. Luo, L. Suo, M.A. Schroeder, K. Xu, S.B. Lee, G.W. Rubloff, C. Wang, Enhancing the reversibility of Mg/S battery chemistry through Li^+ mediation, J. Am. Chem. Soc. 137 (2015) 12388 12393.
[13] B.P. Vinayan, Z. Zhao-Karger, T. Diemant, V.S.K. Chakravadhanula, N.I. Schwarzburger, M.A. Cambaz, R.J. Behm, C. Kübel, M. Fichtner, Performance study of magnesium sulfur battery using a graphene based sulfur composite cathode electrode and a non-nucleophilic Mg electrolyte, Nanoscale 8 (2015) 3296 3306.
[14] J.G. Speight, *Lange's* Handbook of Chemistry, sixteenth ed., McGraw-Hill, New York, 2005.
[15] R. Cooper, J.V.J. Culka, Interchalcogen compounds—I: the sulphur-selenium system, Inorg. Nucl. Chem. 29 (1967) 1217 1224.
[16] R. Steudel, R. Laitinen, Top. Curr. Chem. 102 (1982) 177.
[17] A. Abouimrane, D. Dambournet, K.W. Chapman, P.J. Chupas, W. Weng, K. Amine, A new class of lithium and sodium rechargeable batteries based on selenium and selenium sulfur as a positive electrode, J. Am. Chem. Soc. 134 (2012) 4505 4508.
[18] C. Yang, S. Xin, Y.-X. Yin, H. Ye, J. Zhang, Y.-G. Guo, An advanced selenium carbon cathode for rechargeable lithium selenium batteries, Angew. Chem. Int. Ed. 52 (2013) 8363 8367.
[19] X. Li, J. Liang, Z. Hou, W. Zhang, Yan Wang, Y. Zhu, Y. Qian, A new salt-baked approach for confining selenium in metal complex-derived porous carbon with superior lithium storage properties, Adv. Funct. Mater. 25 (2015) 5229 5238.
[20] J. Zhang, L. Fan, Y. Zhu, Y. Xu, J. Liang, D. Wei, Yitai Qian, Selenium/interconnected porous hollow carbon bubbles composites as the cathodes of Li Se batteries with high performance, Nanoscale 6 (2014) 12952 12957.
[21] X. Li, J. Liang, K. Zhang, Z. Hou, W. Zhang, Yongchun Zhu, Y. Qian, Amorphous S-rich $S_{1\ x}Se_x/C$ ($x \leq 0.1$) composites promise better lithium sulfur batteries in a carbonate-based electrolyte, Energy Environ. Sci. 8 (2015) 3181 3186.
[22] J. Zhang, Y. Xua, L. Fan, Y. Zhua, J. Liang, Y. Qian, Graphene encapsulated selenium/polyaniline core shell nanowires with enhanced electrochemical performance for Li Se batteries, Nano Energy 13 (2015) 592 600.
[23] C.-P. Yang, Y.-X. Yin, Y.-G. Guo, Elemental selenium for electrochemical energy storage, J. Phys. Chem. Lett. 6 (2015) 256 266.
[24] C. Wall, Z. Zhao-Karger, M. Fichtner, Corrosion resistance of current collector materials in bisamide based electrolyte for magnesium batteries, ECS Electrochem. Lett. 4 (2014) C8 C10.
[25] R. Keller, W.B. Holzapfel, H. Schulz, Effect of pressure on the atom positions in Se and Te, Phys. Rev. B 16 (1977) 4404 4412.
[26] N.N. Greenwood, A. Earnshaw, Chemistry of the Elements (2nd ed.), 1997, pp. 751 752.
[27] Y. Cui, A. Abouimrane, J. Lu, T. Bolin, Y. Ren, W. Weng, C. Sun, V.A. Maroni, S.M. Heald, K. Amine, (De)Lithiation mechanism of Li/SeSx (x 0 7) batteries determined by in situ synchrotron x-ray diffraction and x-ray absorption spectroscopy, J. Am. Chem. Soc. 135 (2013) 8047 8056.
[28] M. Shenasa, S. Sainkar, D. Lichtman, XPS study of some selected selenium compounds, J. Electron. Spectrosc. Relat. Phenom. 40 (1986) 329 337.
[29] E. Agostinelli, C. Baistooni, D. Fiorani, G. Mattogno, M. Nogues, An XPS study of the electronic structure of the $ZnxCd_{1\ x}Cr_2$(X S, Se) spinel system, J. Phys. Chem. Solids 50 (1989) 269 272.
[30] R. Inoue, M. Kitagawa, T. Nishigaki, D. Morita, K. Ichino, H. Kusano, H. Kobayashi, XPS study of $Zn_xMg_{1\ x}S$: Mn ternary compound thin films, Appl. Surf. Sci. 142 (1999) 341 345.
[31] G. Lucovsky, A. Mooradian, W. Taylor, G.B. Wright, R.C. Keezer, Identification of the fundamental vibrational modes of trigonal, α monoclinic and amorphous selenium, Solid State Commun. 5 (1967) 113 117.
[32] S.N. Yannopoulos, K.S. Andrikopoulos, On the formation of isolated Se8 rings in zeolites, J. Chem. Phys. 121 (2004) 4747 4758.
[33] A. Goldbach, L.E. Iton, M.-L. Saboungi, Chem. Phys. Lett. 281 (1997) 69 73.
[34] K.E. Murphy, B.B. Wunderlich, B. Wunderlich, Effect of structure on the electrical conductivity of selenium, J. Phys. Chem. 86 (1982) 2827 2835.